SLAC–PUB–5098
September 1989
(T/E)

Shadowing and Anti-Shadowing of Nuclear Structure Functions*

STANLEY J. BRODSKY AND HUNG JUNG LU

Stanford Linear Accelerator Center,
Stanford University, Stanford, California 94309

ABSTRACT

The observed shadowing and anti-shadowing phenomena of quark structure functions in nuclei at small x are interpreted as a consequence of an anti-quark-nucleus multi-scattering process.

Submitted to *Physical Review Letters.*

* Work supported by Department of Energy contract DE–AC03–76SF00515.

One of the most striking nuclear effects seen in the deep inelastic structure functions is the depletion of the effective number of nucleons F_2^A/F_2^N in the region of low x. The results from the EMC collaboration[1] indicate that the effect is roughly Q^2-independent; that is, shadowing is leading twist in the operator product analysis. In contrast, the shadowing of the real photo-absorption cross section due to ρ-dominance [3-6] falls away as an inverse power of Q^2.

Shadowing is a destructive interference effect which causes a diminished flux and interactions in the interior and back face of the nucleus. The Glauber analysis[7] of hadron-nucleus scattering corresponds to the following: the incident hadron scatters elastically on a nucleon N_1 on the front face of the nucleus. At high energies, the phase of the amplitude is imaginary. The hadron then propagates through the nucleus to nucleon N_2, where it interacts inelastically. The accumulated phase of the hadron propagator is also imaginary, so that this two-step amplitude is coherent and opposite in phase to the one-step amplitude where the beam hadron interacts directly on N_2 without initial-state interactions. Thus the target nucleon N_2 sees less incoming flux: it is shadowed by elastic interactions on the front face of the nucleus. If the hadron-nucleon cross section is large, then for large A the effective number of nucleons participating in the inelastic interactions is reduced to $\sim A^{2/3}$, the number of surface nucleons.

In the case of virtual photo-absorption, the photon converts to a $q\overline{q}$ pair at a distance before the target proportional to $\omega = x^{-1} = 2p \cdot q/Q^2$ in the laboratory frame.[8] In a physical gauge, such as the light-cone $A^+ = 0$ gauge, the final-state interactions of the quark can be neglected in the Bjorken limit, and effectively only the anti-quark interacts. The nuclear structure function F_2^A producing quark q can then be written as an integral [9,10] over the inelastic cross section $\sigma_{\overline{q}A}(s')$ where s' grows as $1/x$ for fixed space-like anti-quark mass. Thus, the A-dependence of the cross section mimics the A-dependence of the $\overline{q}$ cross section in the nucleus. We have applied the standard Glauber multi-scattering theory to $\sigma_{\overline{q}A}$, assuming that formalism can be taken over to off-shell $\overline{q}$ interactions (the shadowing mechanism is illustrated in Fig. 1). Our results show that for reasonable values of the $\overline{q}$-nucleon

cross section, one can understand the magnitude of the shadowing effect at small x. Moreover, if one introduces an $\alpha_R \simeq 1/2$ Reggeon contribution to the $\overline{q}N$ amplitude, the real phase introduced by such a contribution automatically leads to "anti-shadowing" (effective number of nucleons $F_2^A(x,Q^2)/F_2^N(x,Q^2) > A$) at $x \simeq 0.15$ of the few percent magnitude revealed by the SLAC and EMC experiments.[1,2]

Our analysis provides the input or starting point for the log Q^2 evolution of the deep inelastic structure functions, as given for example by Mueller and Qiu.[11] The parameters for the effective $\overline{q}$-nucleon cross section required to understand shadowing phenomena provide important information on the interactions of quarks in nuclear matter.

Our analysis also has implications of the nature of particle production for virtual photo-absorption in nuclei. At high Q^2 and $x > 0.3$, hadron production should be uniform throughout the nucleus. At low x or at low Q^2, where shadowing occurs, the inelastic reaction occurs mainly at the front surface. These features can be examined in detail by studying non-additive multi-particle correlations in both the target and current fragmentation region.

Recently, Frankfurt and Strikman have proposed a model for the shadowing and anti-shadowing of the leading-twist nuclear structure function in the small x region.[12] Their approach differs with ours in two ways: (1) They apply the Glauber's formula in the spirit of a vector meson dominance calculation in an aligned jet model, hence their analysis essentially aims toward the lower Q^2 region ($Q^2 \leq 4$ GeV^2); and (2) The anti-shadowing effect is required on the basis of the momentum sum rule rather than attributed to any particular dynamical mechanism.

We shall neglect the quark spin degrees of freedom in our analysis. The distribution functions of spinless partons in the nucleon and nucleus are, respectively[9,10]:

$$xf^N(x) = \frac{2}{(2\pi)^3}\frac{Cx^2}{1-x}\int ds d^2k_\perp \ \mathrm{Im}\ T_R^N(s,\mu^2) \qquad (1)$$

and

$$xf^A(x) \;=\; \frac{2}{(2\pi)^3}\frac{Cx^2}{1-x}\int dsd^2k_\perp \;\mathrm{Im}\; T_R^A(s,\mu^2) \tag{2}$$

where the integral is over the right-hand cut of the forward $\overline{q}$-nucleon (or $\overline{q}$-nucleus) scattering amplitude Im $T_R^N(s,\mu^2)$ (Im $T_R^A(s,\mu^2)$), which includes the propagators of the partons. We will assume the amplitudes vanish rapidly as $\mu^2 \to -\infty$, where

$$\mu^2 \;=\; -x(s+k_\perp^2)/(1-x) + xM^2 - k_\perp^2 \tag{3}$$

is the invariant four-momentum squared of the interacting parton. The constant C incorporates the parton wavefunction renormalization constant,[10] M is the mass of nucleon, and $k_\perp$ is the parton's transverse momentum.

The scaled effective number of nucleons for fixed x is defined as ($\nu^2 = -\mu^2$)

$$\begin{aligned} A_{eff}(x)/A \;&=\; F_2^A(x)/AF_2^N(x) \;=\; xf^A(x) \;/\; Axf^N(x) \\ &=\; \int dsd^2k_\perp \;\mathrm{Im}\; T_R^A(s,\nu^2) \;\Big/\; A\int dsd^2k_\perp \;\mathrm{Im}\; T_R^N(s,\nu^2) \end{aligned} \tag{4}$$

We have implicitly considered an "average parton," that is, $f^A(x)$ and $f^N(x)$ are the distribution functions averaged over all the quark and anti-quark flavors. The region of integration transformed onto the $s-\nu^2$ plane is indicated on Fig. 2, where $\overline{\nu}^2$ represents the typical cutoff in the ν^2 dependence of the amplitude T_R^N (or T_R^A) and s^* is the first threshold in the s-cut of the amplitude T_R^N. Observe that when $x \to 0$, the main contribution to the integrals comes from the region of large s and finite ν^2, whereas the case $x \to 1$ probes into the low-s and large-ν^2 sector.

In general, we expect the $\overline{q}-A$ scattering amplitude can be obtained from the $\overline{q}-N$ amplitude via Glauber's theory.[13] For our model, we also include $\alpha_R = 1/2$ and $\alpha_R = -1$ Reggeon terms, in addition to the Pomeron exchange term [the diagram corresponding to these contributions is shown on Fig. 1(b)]:

$$T_{\overline{q}N}(s,\nu^2) \;=\; \sigma[is\beta_1(\nu^2) + (1-i)s^{1/2}\beta_{1/2}(\nu^2) + is^{-1}\beta_{-1}(\nu^2)] \tag{5}$$

(Note: this is the amputated $\overline{q}-N$ amplitude, i.e., by attaching the external parton propagators to $T_{\overline{q}N}$, we recover the non-amputated amplitude T_R^N.) For large s, the Pomeron term dominates and $T_{\overline{q}N}$ becomes imaginary, thus leading

to the shadowing effect for small x. However, at lower values of s the real part is important, and we shall see this leads to an anti-shadowing enhancement of the $\overline{q}-A$ amplitude. The main role of the $\alpha_R = -1$ "Reggeon" in the parametrization (5) is to simulate the valence quark contribution of the nucleon in the low x domain. Further terms can be added, but these three terms reflect the essential properties of parton distribution functions needed here to study the low x region (see Fig. 3).

We assume a Gaussian wavefunction for the nucleons in the nucleus[14–16]:

$$\begin{aligned} \left|\Psi(\mathbf{r}_1,\cdots,\mathbf{r}_A)\right|^2 &= \prod_{j=1}^{A}(\pi R^2)^{3/2}\ \exp(-\mathbf{r}_j^2/R^2) \\ R^2 &= \frac{2}{3}R_0^2\ ;\quad R_0\ =\ 1.123A^{1/3}\ fm \end{aligned} \tag{6}$$

and adopt the usual parametrization for the high energy particle-nucleon scattering amplitude

$$T_{\overline{q}N}(s,\nu^2,\mathbf{q})\ =\ T_{\overline{q}N}(s,\nu^2)\ \exp(-\frac{1}{2}b\mathbf{q}^2) \tag{7}$$

where $\mathbf{q}^2 \simeq -q^2$ is the square of the transferred momentum in the lab frame.

The Glauber's analysis[14–16] yields[17]

$$T_{\overline{q}A}(s,\nu^2)\ =\ T_{\overline{q}N}(s,\nu^2)\sum_{j=1}^{A}\frac{1}{j}\binom{A}{j}\left\{\frac{iT_{\overline{q}N}(s,\nu^2)}{4\pi p_{cm}s^{1/2}(R^2+2b)}\right\}^{j-1} \tag{8}$$

After attaching the propagators to the amplitudes in Eqs. (5) and (8), the ratio

$$\frac{A_{eff}(x)}{A}\ =\ \frac{\int ds\ d^2k_\perp\ \mathrm{Im}\ T_{\overline{q}A}(s,\nu^2)\Delta_F^2(\nu^2)}{A\int ds\ d^2k_\perp\ \mathrm{Im}\ T_{\overline{q}N}(s,\nu^2)\Delta_F^2(\nu^2)} \tag{9}$$

can be evaluated numerically.

We shall assume that $T_{\overline{q}N}(s,\nu^2)$ vanishes as the inverse power of ν^2 at large space-like quark mass. We take

$$\beta_\alpha(\nu^2)\ =\ \frac{f_\alpha}{1+(\nu^2/\overline{\nu}_\alpha^2)^{n_\alpha}}\quad , \tag{10}$$

where $\alpha = 1, 1/2, -1$. The characteristic scale for the Pomeron and the $\alpha_R = 1/2$ Reggeon is taken to be: $\overline{\nu}_1^2,\ \overline{\nu}_{1/2}^2 \simeq 0.30$ GeV^2. The $\alpha_R = -1$ valence term is assumed to fall off at the nucleon mass scale: $\overline{\nu}_{-1}^2 \simeq 1$ GeV^2. In order to give a

short-momentum range behavior to the Pomeron and the $\alpha_R = 1/2$ Reggeon, we fix $n_1, n_{1/2} = 4$, and we assign $n_{-1} = 2$ to provide the long tail necessary for larger x behavior of the valence quark distribution function. By definition $f_1 = 1$, whereas $f_{1/2}$ and f_{-1} are adjusted consistently with the shape of the nucleon structure function at low x. The propagator of the anti-quark lines in the non-amputated amplitudes is assumed to have a monopole form on the space-like quark mass:

$$i\Delta_F(\nu^2) \propto \frac{1}{\overline{\nu}_p^2 + \nu^2} \quad . \tag{11}$$

A summary of the set of parameters used is given in Table I. The resulting nucleon structure function computed from Eq. (1) is shown in Fig. 3. The parametrization used for $T_{\overline{q}N}$ gives a reasonable description of the components of F_2^N at low x.

We can now compute the nuclear structure function and the ratio $A_{eff}(x)/A$ from Eq. (9). The results are given in Fig. 4 for $A = 12$, 64, and 238. One observes shadowing below $x \simeq 0.1$ and an anti-shadowing peak around $x \simeq 0.15$. The shadowing effects depend roughly logarithmically on the mass number A. The magnitude of shadowing predicted by the model is consistent with the data for $x > 0.01$; below this region, one expects higher-twist and vector-meson dominance shadowing to contribute. For $x > 0.2$ other nuclear effects must be taken into account. Most of the parameters used in the model are assigned typical hadronic values, but σ and $f_{1/2}$ deserve more explanation. Here, σ controls the magnitude of shadowing effect near $x = 0$: a larger value of σ implies a larger $\overline{q}^* N$ cross section and thus more shadowing. Notice that σ is the effective cross section at zero $\overline{q}$ virtuality, thus the typical value $\langle\sigma\rangle$ entering the calculation is somewhat smaller than σ. A variation in the parameter $f_{1/2}$ modifies the amount of anti-shadowing by altering the real-to-imaginary-part ratio of the scattering amplitude.

Our semi-quantitative analysis shows that parton multiple-scattering process provides a mechanism for explaining the observed shadowing at low x in the EMC–SLAC data. The existence of anti-shadowing requires the presence of regions where the real part of the $\overline{q} - N$ amplitude dominates over the imaginary part.

Finally, we note that due to the perturbative QCD factorization theorem for inclusive reactions, the same analysis can be extended to Drell–Yan processes. Thus shadowing and anti-shadowing should also be observable in the nuclear structure function $F_2^A(x_2, Q^2)$ extracted from massive lepton pair production on nuclear target[18] at low x_2.

REFERENCES

[1] J. Ashman *et al., Phys. Lett.* **202B**, 603 (1988) and CERN-EP/88-06 (1988) M. Arneodo *et al., Phys. Lett.* **211B**, 493 (1988).

[2] R. G. Arnold *et al., Phys. Rev. Lett.* **52**, 727 (1984) and SLAC-PUB-3257 (1983).

[3] J. S. Bell, *Phys. Rev. Lett.* **13**, 57 (1964).

[4] L. Stodolsky, *Phys. Rev. Lett.* **18**, 135 (1967).

[5] S. J. Brodsky and J. Pumplin, *Phys. Rev.* **182**, 1794 (1969).

[6] J. J. Sakurai and D. Schildknecht, *Phys. Lett.* **40B**, 121 (1972); *ibid.*, **41B**, 489 (1972); *ibid.*, **42B**, 216 (1972).

[7] R. J. Glauber, *Lectures in Theoretical Physics*, edited by W. E. Brittin *et al.*, (Interscience, New York, 1959) vol. I.

[8] T. H. Bauer *et al., Rev. Mod. Phys.* **50**, 261 (1978).

[9] P. V. Landshoff, J. C. Polkinghorne and R. D. Short, *Nucl. Phys.* **B28**, 225 (1971).

[10] S. J. Brodsky, F. E. Close and J. F. Gunion, *Phys. Rev.* **D5**, 1384 (1972).

[11] A. H. Mueller and J. Qiu, *Nucl. Phys.* **B268**, 427 (1986); J. Qiu, *Nucl. Phys.* **B291**, 746 (1987).

[12] L. L. Frankfurt and M. I. Strikman, *Nucl. Phys.* **B316**, 340 (1988) and *Phys. Rep.* **160**, 235 (1988).

[13] Rigorously, we should also include the effect due to the shadowing of the gluon structure function of the nucleus. A more detailed analysis may be able to distinguish quark and gluon shadowing effects.

[14] V. Franco, *Phys. Rev. Lett.* **24**, 1452 (1970) and *Phys. Rev.* **C6**, 748 (1972).

[15] A. Y. Abul-Magd, *Nucl. Phys.* **B8**, 638 (1968).

[16] R. A. Rudin, *Phys. Lett.* **30B**, 357 (1969).

[17] The relationship between the invariant amplitude $T_{\bar{q}N}$ and the lab frame amplitude $F_{\bar{q}N}$ is given by

$$F_{\bar{q}N}(k,\nu^2,\mathbf{q}) \;=\; \frac{k}{8\pi p_{cm}\sqrt{s}}\, T_{\bar{q}N}(s,\nu^2,\mathbf{q}) \quad ,$$

and the optical theorem reads:

$$\sigma_{tot} \;=\; \frac{4\pi}{k}\,\mathrm{Im}\; F_{\bar{q}N}(k,\nu^2,\mathbf{0}) \;=\; \frac{1}{2p_{cm}\sqrt{s}}\,\mathrm{Im}\; T_{\bar{q}N}(k,\nu^2,\mathbf{0}) \quad ,$$

where k is the virtual quark's 3-momentum in the lab frame,

$$p_{cm} \;=\; [\;\nu^2 + (s - M^2 - \nu^2)^2/4s\;]^{1/2}$$

is the 3-momentum in the quark-nucleon center-of-mass energy system, and M is the nucleon mass.

[18] E. L. Berger, *Nucl. Phys.* **B267**, 231 (1986).

Table I Value of parameters used in the multi-scattering model.

σ	30 mb	$f_{1/2}$	0.90 GeV
$\overline{\nu}_1^2, \overline{\nu}_{1/2}^2, \overline{\nu}_p^2$	0.30 $(\mathrm{GeV})^2$	f_{-1}	0.20 $(\mathrm{GeV})^4$
$\overline{\nu}_{-1}^2$	1.00 $(\mathrm{GeV})^2$	M^2	0.88 $(\mathrm{GeV})^2$
$n_1, n_{1/2}$	4	s^*	1.52 $(\mathrm{GeV})^2$
n_{-1}	2	b	10 $(\mathrm{GeV/c})^{-2}$

FIGURE CAPTIONS

1) (a) The double-scattering amplitude that shadows the direct interaction of the anti-quark with N_2. (b) The same mechanism as in (a), drawn in the traditional "handbag" form. The Pomeron and Reggeon exchanges between the quark line and N_1 are explicitly illustrated.

2) The region of integration of the amplitudes T_R^N and T_R^A in the $s - \nu^2$ plane.

3) The computed nucleon structure function $F_2(x)$ assuming the set of parameters in Table I and normalized such that $F_2(0) = 1$. In order to show separate sea distribution $xS(x)$ and valence distribution $xV(x)$, we have assumed the parametrization:

$$\begin{aligned} T_{\bar{q}N}^{sea}(s,\nu^2) &= \sigma[is\beta_1(\nu^2) + 1.2(1-i)s^{1/2}\beta_{1/2}(\nu^2)] \\ T_{\bar{q}N}^{valence}(s,\nu^2) &= \sigma[-0.2(1-i)s^{1/2}\beta_{1/2}(\nu^2) + is^{-1}\beta_{-1}(\nu^2)] \quad . \end{aligned}$$

4) The predicted ratio of $A_{eff}(x)/A$ of the multi-scattering model in the low x region for different nuclear mass number. The data points are results from the EMC experiment for Cu and Ca.

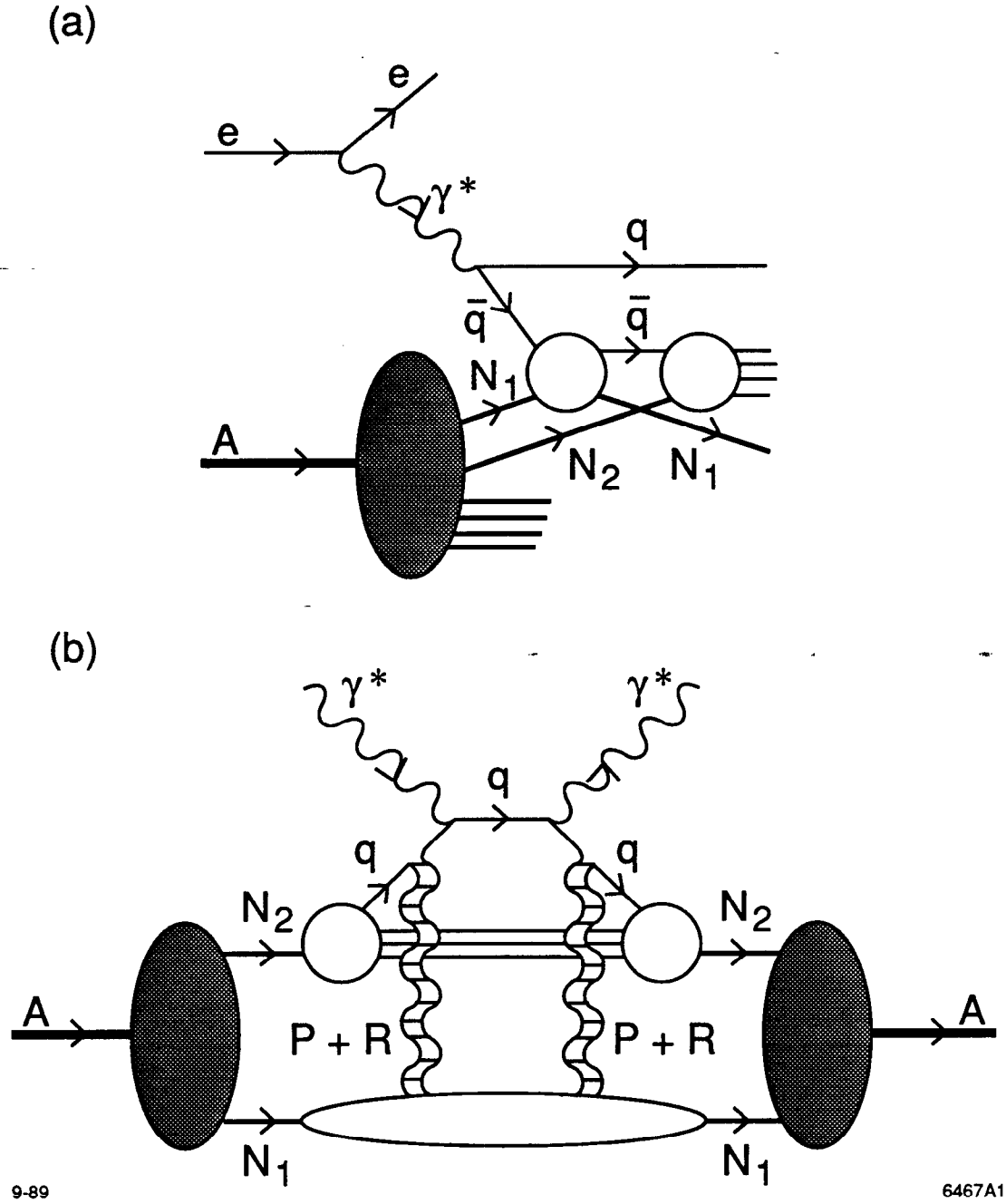

Fig. 1

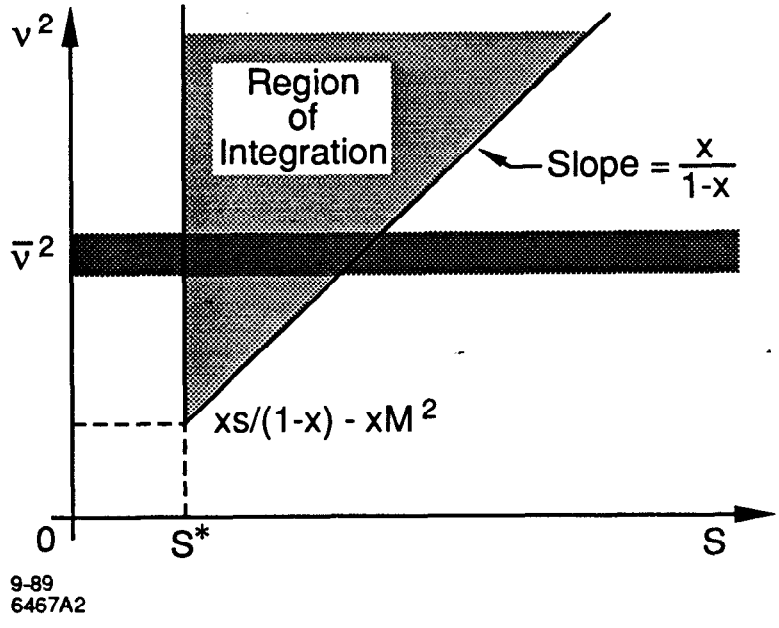
ν^2
Region of Integration
Slope = $\frac{x}{1-x}$
$\bar{\nu}^2$
$xs/(1-x) - xM^2$
0
S*
S
9-89
6467A2

Fig. 2

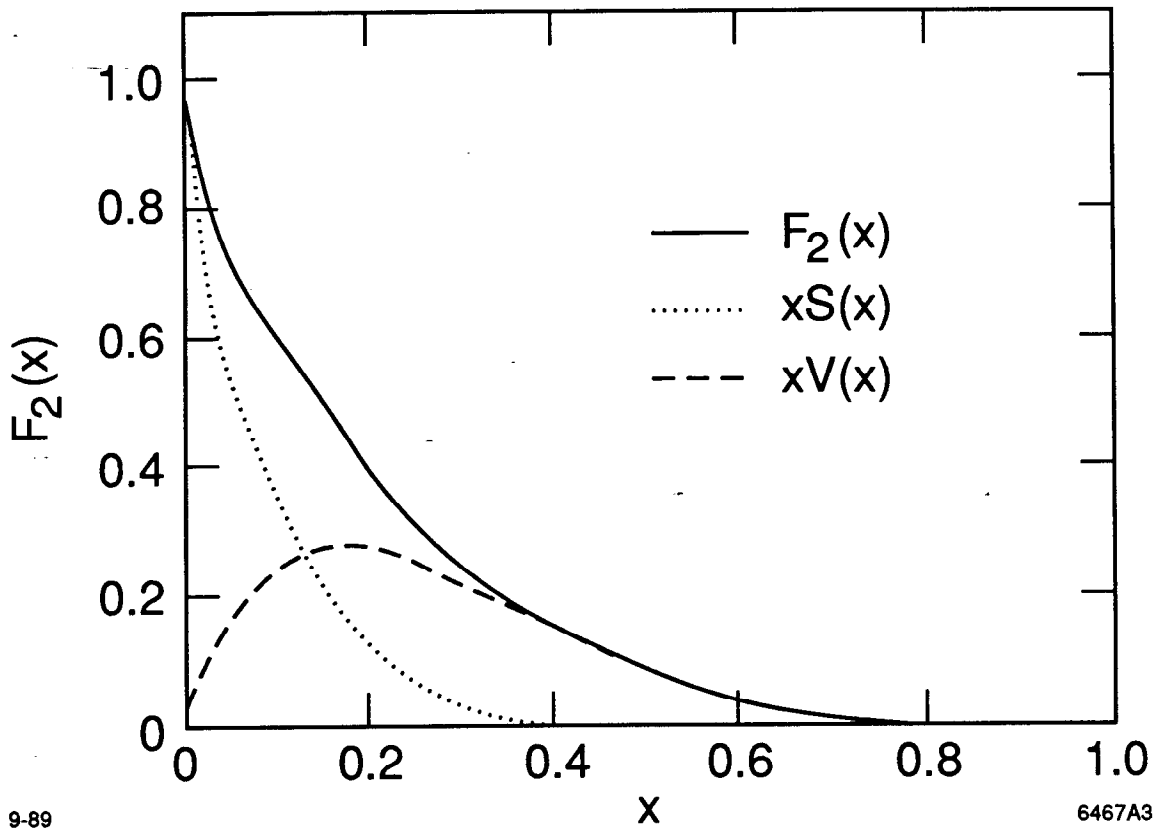

Fig. 3

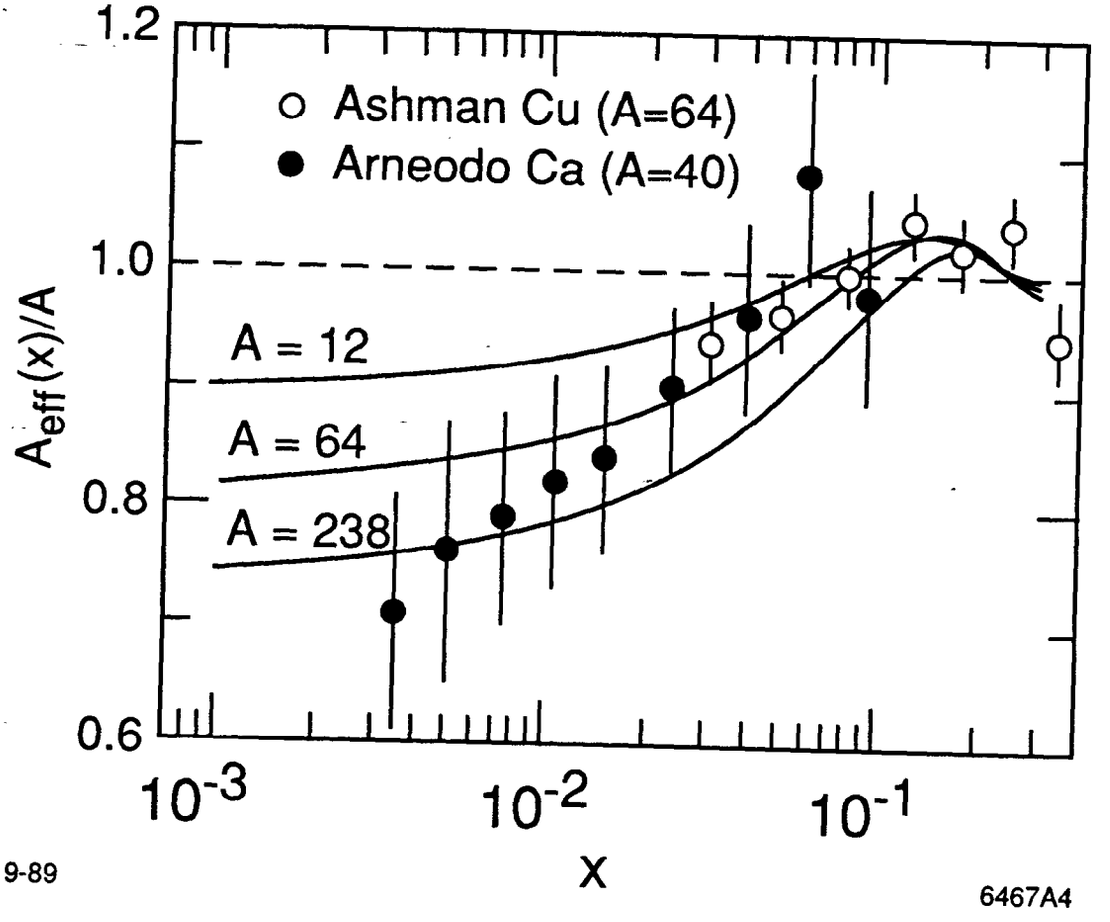
1.2
1.0
0.8
0.6
Ashman Cu (A=64)
Arneodo Ca (A=40)
A = 12
A = 64
A = 238
$A_{eff}(x)/A$
10^{-3}
10^{-2}
10^{-1}
X
9-89
6467A4

Fig. 4